

CERN LIBRARIES, GENEVA



SC00000157

CERN/DRDC 93-3

DRDC/P-46

January 13, 1993

SCP
CERN-DRDC
93-3

R&D proposal

DEVELOPMENTS FOR A SCINTILLATOR TILE SAMPLING HADRON CALORIMETER WITH "LONGITUDINAL" TILE CONFIGURATION

M. Bosman, M. Cavalli-Sforza, F. Teubert
IFAE, Universitat Autònoma de Barcelona, Barcelona, Spain

C. Blaj, V. Boldea, S. Dita
Institute for Atomic Physics, Bucharest, Romania

Z. Ajaltouni, F. Badaud, N. Bouhemaïd, P. Brette, M. Brossard, R. Chadelas,
J-C. Chevaléyre, M. Crouau, F. Daudon, J-J. Dugne, B. Michel, G. Montarou,
G.S. Muanza, D. Pallin, L-P. Says, F. Vazeille
LPC, Clermont-Ferrand, France

O. Gildemeister¹, M. Nessi, L. Poggioli, P. Sonderegger
CERN, Geneva, Switzerland

A. Amorim, P. Ferreira, A. Gomes, A. Henriques², A. Maio, L. Peralta
LIP and University of Lisbon, Lisbon, Portugal

R. Leitner, M. Suk
Prague, Czechoslovakia

M. Kostrikov, M. Kulagin, V. Lapin, Y. Protopopov, A. Solodkov, A. Zaitsev
IHEP, Protvino, Russia

H. Hakopian
Yerevan, Armenia

¹Spokesperson

²Also at CERN

Abstract

In a scintillator tile calorimeter with wavelength shifting fiber readout significant simplifications of the construction and the assembly are possible if the tiles are oriented "longitudinally", i.e. in $r-\phi$ planes for a barrel configuration. For a hybrid calorimeter consisting of a scintillator tile hadron compartment and a sufficiently containing liquid argon electromagnetic (EM) compartment, as proposed for the ATLAS detector, good jet resolution is predicted by simulations, which is not affected by this particular orientation of the tiles.

The aim of the proposed development program is to construct a calorimeter test module with longitudinal tiles and to check the simulation results by test beam measurements. In addition several component tests and further simulations and engineering studies are needed to optimize the design of a large calorimeter structure to be used in collider experiments. The construction of a test module will also provide valuable experience for the design of a large system.

Contents

1	Introduction	4
2	Arguments for the longitudinal configuration	4
3	The ATLAS hybrid calorimeter option	5
3.1	The proposed structure of the barrel part	5
3.2	Scintillator tiles	6
3.3	WLS fibers	6
3.4	Light detectors	7
3.4.1	Active area of light detectors	7
3.4.2	PMTs	7
3.4.3	APDs	7
3.5	Radiation hardness	8
3.6	Calibration and monitoring	8
4	Simulation results	8
4.1	Energy resolution and linearity of the response	9
4.2	Effect of dead materials	10
5	Proposed parameters of a test module	10
6	The R&D Program	11
6.1	Construction of the calorimeter test module	11
6.2	Preparation of the test beam setup and beam tests	11
6.3	Light detector testing and developments	11
6.4	Light detector mounting scheme	12
6.5	Simulation program	12
6.6	Component tests and radiation damage studies	12
6.7	Engineering studies	12
6.8	Time scale	13
6.9	Budget	13
6.10	Sharing of responsibilities	13

1 Introduction

Scintillator calorimeters are widely used in high energy physics experiments. They offer good performance and fast readout at relatively low cost. The readout of the tiles by means of wavelength shifting (WLS) fibers is being used in the CDF experiment [1], and is planned for SDC [2] and leads to an excellent hermeticity of the detector, particularly important in collider experiments. In presently existing and proposed calorimeter configurations the scintillator tiles are oriented about normal to the particle trajectories. Simulations indicate that inside a hadron calorimeter, having an about 1.5 to 2 interaction lengths (λ_I) thick EM compartment in front, the orientation of the scintillator tiles with respect to the direction of the primary particles does not affect the energy resolution for hadrons or jets provided the tiles are staggered in depth. The staggering assures a good sampling homogeneity and avoids too long particle track segments within the scintillator material.

In a layout proposed for the ATLAS detector the scintillator tiles and absorber plates of the hadron calorimeter are oriented in r - ϕ planes in the barrel part, and in ϕ - z planes in the end-plugs. This geometry simplifies both the construction of the iron absorber part and the routing of the WLS-fibers, which in the barrel run straight in radial direction, coupling to the ϕ -edges of the scintillator plates. It also offers a relatively simple assembly procedure. A hadron calorimeter of this configuration combined with a liquid argon EM part is retained by the ATLAS collaboration as the only alternative to a full liquid argon option.

2 Arguments for the longitudinal configuration

In scintillator tile calorimeters the conventional tile orientation in planes normal to the particle trajectories complicates the readout with WLS-fibers. For an efficient optical tile-fiber coupling each fiber has to run in the plane of the corresponding tile. To combine all signals from towers, however, the fibers need complicated, curved routings inside the active volume of the detector (Fig. 1a). In addition the absorber plates, being separated by the tiles, need to be linked to each other in order to be externally supported. Both these complications are avoided by putting the tiles into a longitudinal position [3]. The fibers, coupling to the edges of the tiles, run entirely in longitudinal direction (Fig. 1b), and the absorber planes are longitudinal as well and can easily be supported from outside. In addition the fact that the absorber plates in barrel sectors have equal shapes offers economic manufacturing procedures (punching).

Preliminary tests have shown that an efficient optical coupling of the WLS-fibers to the edges of the tiles can be achieved if the thickness of the tiles does not exceed three times the diameter of the fibers. To avoid long particle track segments inside the scintillator material, the individual tiles can be kept short in longitudinal direction, and in successive layers the tiles can be staggered (Fig. 2). That in this case the energy resolution of hadrons or jets is not degraded, has been checked by simulations. A proposal for the hadron part of a hybrid calorimeter for the ATLAS detector is based on these ideas.

3 The ATLAS hybrid calorimeter option

A description of the hybrid calorimeter with a scintillating tile hadron compartment proposed for the ATLAS detector is given in the ATLAS Letter of Intent [4]. The EM compartment consists of a lead-liquid argon calorimeter which, together with the superconducting solenoid coil and the cryostat material, represents about $2 \lambda_I$ at zero rapidity. In the present design the hadron compartment consists of a barrel part of 6.8 m length and two endcaps (Fig. 3). The endcaps have an outer part ("extended barrel") covering the radial range of the barrel and having a corresponding configuration. The inner parts of the endcaps have the form of plugs, consisting of azimuthal sector modules with the tiles and absorber plates in ϕ - z planes. The granularity is chosen to be 0.1×0.1 in the η and ϕ directions within the η -range of ± 2.4 . Beyond this interval it is 0.2×0.2 .

In the following the barrel part will be described in detail. The end-plugs are based on the same concept, but require further engineering studies.

3.1 The proposed structure of the barrel part

The barrel hadron calorimeter is subdivided into 64 independent sector modules of the full barrel length of 6.8 m (Fig. 4). The width of each sector corresponds to the azimuthal granularity of 0.1. Therefore, the scintillator tiles traverse the width of the module, and all WLS-fibers, coupling to both ϕ -edges of the tiles, are accessible from the side faces of each module. The tiles and fibers are oriented in radial direction. This leads to a nonpointing geometry for nonzero rapidity. A fourfold segmentation in depth allows, however, to form pseudopointing towers from the rectangular cells (Fig. 5). This cell structure offers also for the readout an up to fourfold segmentation in depth. But for economic reasons one may as well prefer to combine the readout of subsequent cells into a common photodetector channel. Furthermore in the last layer where the granularity is less critical, adjacent cells could be combined. The size of the individual tiles in radial direction is chosen to be 100 mm for the innermost of the four layers of cells and might be increased for the outer layers. The layers of tiles are staggered with respect to each other. For each cell (or combination of cells), except perhaps of the last layer, it is foreseen to read out the tiles from both ϕ edges independently. This offers redundancy for the case of individual channels failures, and the possibility of offline corrections in cases of asymmetric "left/right" responses.

Since the absorber structure of each barrel sector module consists of a large number of trapezoidal steel plates of the same shape, these plates will most economically be produced by punching. This procedure favours plate thicknesses around 1.5 to 2 mm. The whole absorber structure of a sector module will thus be a stack of thin trapezoidal plates, partly of full size, partly interrupted radially to leave the slots for the introduction of the scintillator tiles. The whole stack is compressed by means of a series of rods traversing the absorber stack and the tiles over the whole length of the sector module (see Fig. 4).

In the present design the tile thickness is 3 mm with a fiber diameter of 1 mm. The absorber thickness between two adjacent tiles of the same layer is 13.6 mm, built up of plates of 1.7 mm. This leads, together with a 0.4 mm margin for sliding the tiles into the slots, to a tile to tile pitch of 17 mm. The active depth of the modules in radial direction is 180 cm. This corresponds to about $9 \lambda_I$ at $\eta = 0$.

The steel plate structure continues in the radial direction by another 10 cm beyond the active region of the barrel sector. On the outer face of the compressed stack a strong steel profile will be welded, which will give rigidity to the structure and at the same time support the light detectors. This steel profile, together with the 10 cm of passive stack structure, will also act as a return yoke for the magnetic field of the central solenoid. A light steel plate will also be welded to the entrance face of the absorber stack to allow the temporary mounting of manipulation devices. Only after the completion of the absorber structure of each module with its welded members the scintillator tiles will be introduced (by recessing the corresponding rods). The last step is the mounting of the WLS-fibers and of the light detectors.

During installation all sectors of the barrel will be linked one to the other in sequence and will form a self-supporting structure resting on legs or rails.

3.2 Scintillator tiles

The tiles will be made of polystyrene based plastic scintillator material. They might either be cut out of large plates commercially available, or be produced by an injection moulding procedure developed at IHEP, Protvino, to be used in other experiments [5]. The latter method is the more economic one, as these tiles are produced from a mixture of granulated polystyrene with primary and secondary dopants at a rate of 1 to 2 minutes per tile. The mould can be of arbitrary shape, providing the tiles with grooves and holes as required. In general no additional mechanical treatment (e.g. polishing) is needed. The dyes and their concentration can be chosen to achieve the best light yield for the combination of the scintillator tile and the WLS-fiber. Some additional R&D will be required for the mould design and the scintillator composition.

The edges of the tiles coupling to the fibers need optimized shaping. For an efficient optical coupling of 3 mm scintillator plates to 1mm diameter readout fibers the scheme of Fig. 6 has been tested. The fiber is air-coupled to a 1 mm groove cut into the narrow face of the plate, the adjacent edges of which are cut at 45 degrees and polished. A comparative measurement gave 70 % light yield with respect to a standard 2 mm WLS plate (as used in the UA2 endcap calorimeter) coupled to a flat edge of the same scintillator plate. The rear end of the 2 m long fiber was Aluminium plated, while the WLS plate had a white paint on the rear edge. Further studies are envisaged to optimize this shaping with respect to the efficiency, reproducibility, and stability of the light collection as well as to the manufacturing procedure.

3.3 WLS fibers

The WLS fibers transform the blue light from the scintillators to the green region of the spectrum (peaked at about 480 nm). Radiation hard fibers made of polystyrene base material with appropriate dopings are available from several companies. The decay time constant of the light emission is of the order of 10 ns. The light attenuation length is about 2 m, if measured at a distance between one and two meters from the light detector. All fibers will, at their rear end, receive a reflective Al-layer by a sputtering procedure. The reflectivity is typically around 85 %. This mirror reduces the response variation over the active length of the fiber (30 to 50 cm) to less than 5 %. Fig. 7 shows a typical dependence of the response (log scale) of a fiber as a function of

the distance between the excited region (blue scintillator light) and the light detector. The mirror end of the fiber is at a distance of 2.2 m.

3.4 Light detectors

3.4.1 Active area of light detectors

The number of bunched fibers per cell lays between 24 and 54, for the smallest and the largest cell, respectively (for 4-fold segmentation in depth). These numbers include an additional clear fiber per bunch for light pulser monitoring. The highest value corresponds to a bunch diameter of 8.4 mm.

A light-guide is used to mix the light from every fiber in a given bunch before reaching the light detector. Full simulations, with air gaps before and after the mixer, show that the optimum shape of the mixer is a parallelepiped with dimensions $9 \times 9 \times 14$ mm³.

As a result small size light detectors can be used, which simplifies their protection against stray magnetic fields and may allow a mounting scheme which makes the light detectors more easily accessible, as mentioned in section 6.4.

We consider two options for the light detectors : photo-multiplier tubes (PMTs) and avalanche photo-diodes (APDs).

3.4.2 PMTs

Small 10-stage PMTs, with 3/4 inch diameter or less, are adequate. In the super-conducting air core toroid option of the ATLAS detector, the photo-detectors will be exposed to a stray magnetic field of 0.05 to 0.1 T. PMTs would need carefully designed shielding. First estimates indicate the outer shield should be around three times the diameter of the tube.

3.4.3 APDs

The well known advantages of APDs are : very high quantum efficiency, compactness, very low power consumption, insensitivity to magnetic fields, good speed and intrinsic gain. Recent advances in the fabrication technology of APDs have resulted in commercially available low-noise devices with a sensitive area of 180 mm² [6].

Intensive studies have been performed by the RD1 Collaboration, both on a special test bench and in test beams at CERN (the APDs were used as readout of the RD1 lead/scintillating fiber EM prototype) [7]. When exposed to high energy particles (electrons, muons, pions), the intrinsic properties are kept (e.g. reverse current), and the calorimeter performances are the same as the ones obtained with PMTs (Fig. 8). The APD pulse shape is satisfactory (Fig. 9a), although a bit slower than the PMT one. The speed is retained if the APD is associated with a fast current preamplifier (Fig. 9b).

For the tile calorimeter, smaller APDs (about 60 mm²) can be used, thus gaining on speed (6 ns rise time and 25 ns width as predicted by simulations), signal-to-noise and cost. The high voltage and the temperature have to be well stabilized (to about 0.8 V and 0.2° C respectively).

3.5 Radiation hardness

The radiation damage of a LHC hadron calorimeter is much less critical than the electromagnetic part. Nevertheless, because of the long operation time, this effect should be considered.

The expected doses at the hadron shower maximum are smaller than the doses at the EM shower maximum by a factor of the order of 20 in the barrel and a factor around 5 in the endcap ([4], page 82). For an integrated luminosity of 10^5 pb^{-1} /year maximum dose rates of 0.02 kGy/year and 4 kGy/year are expected in the barrel and in the end-plugs, respectively.

Experimental results obtained so far by irradiating a scintillating tile-lead WLS-fiber EM calorimeter prototype have shown that a signal reduction of around 2% occurs after an irradiation of about 1 kGy [8]. Simulation studies performed for a full scintillator tile WLS-fiber calorimeter indicate that a light loss of 10% induces a constant term of 2% in the single pion energy resolution.

Extrapolating these results it is expected that in the ATLAS hybrid configuration, the barrel hadron compartment will not noticeably be affected for more than 20 years of operation. In the end-plugs, assuming that the EM compartment will not suffer from radiation, the jet energy resolution will not significantly be degraded for about 5 years, even at maximum rapidity. A periodic recalibration, however, will be needed for $|\eta| > 2.5$.

3.6 Calibration and monitoring

The calibration of the whole calorimeter, for which we aim at an accuracy of 2 %, will be based on several methods. A sample fraction of the sector modules will be measured with muons, pions and electrons in a test beam. In parallel a light flasher system and probably a system of movable radioactive sources (e.g. inside the axial rods, see Fig. 4, which could be built as hollow tubes) will provide the monitoring of all channels.

In the final setup, energy flow measurements can cross-calibrate the sectors one to each other. This method measures the average energy deposited from all pp interactions into all cells and can be used to monitor the calorimeter response [9], and, using the ϕ -symmetry, to transfer the absolute test beam calibration of the sample modules to the full calorimeter. It is envisaged that these measurements can be performed during normal runs by integrating the photodetector dc-currents. For nominal luminosity the expected dc-currents are on average about three orders of magnitude above typical PMTs dark currents. The photodetector dark currents can however also be measured independently by integrating the dc-currents over the bunch free periods of the LHC cycle only. By doing this the pure interaction induced currents can be evaluated.

Combining the energy flow measurements with a corresponding integration of a (relative but stable) luminosity signal may also provide information on any overall or η -dependent time drift of the calorimeter calibration.

4 Simulation results

The strength of the design rests on the hypothesis that the specific orientation (longitudinal) of the tiles does not affect the overall hadronic performance. In order to assess this hypothesis the response to hadrons and jets is being studied using the best present

knowledge of the hadronic shower behaviour. The simulations are organized within the GEANT framework, making use of the most recent developments of this package (GEANT 3.15 [10]) and taking advantage of the relatively “easy” layout structure of the proposed detector, which allows a full and detailed geometrical description in GEANT (as presented in section 3.1) while keeping the simulation time reasonable (1 HP 720 sec/GeV). Furthermore, in order to be realistic and to profit from the studies already performed by the ATLAS Collaboration towards a hybrid calorimeter concept, the tile calorimeter has been inserted into the design of the ATLAS detector, accounting for the presence of the field within the solenoid, the liquid argon EM calorimeter and the liquid argon preshower detector (the energy resolution of such an EM section is $10\%/\sqrt{E}$ for electromagnetically interacting particles).

Special care has been given to the description of gaps and of the materials involved in the various interface regions between the solenoidal coil, the preshower detector and the EM accordion calorimeter. Wherever available, existing engineering solutions have been described in the Monte-Carlo.

The breakdown of the materials and gaps in front of the tile calorimeter, as they have been used, are summarized in Table 1 (values at $\eta = 0$). Typically about $2 \lambda_I$ have to be accounted for in the EM section. This implies that on average for a jet of 100 GeV, about 60% of the energy is sampled by the EM section alone. The dead materials in between EM and hadronic (HAD) calorimeter in this model amounts to $0.2 \lambda_I$ or $1.6 X_0$. In particular, the electromagnetic absorption power of these dead materials has been minimized choosing Aluminum for the warm cryostat vessel structure.

The calorimeter performance is studied through full electromagnetic and hadronic shower simulations. All hadronic models available in this version of GEANT have been tested (NUCRIN, GHEISHA, FLUKA). Differences up to 20 – 25% in the value of the sampling term of the energy resolution function are found in the comparison of the results. A choice has been made to use the FLUKA model, which reproduces the experimental data from the SPACAL and RD1 Collaboration [11] in the case of a scintillating fibre detector and from the ZEUS Collaboration for tiles [12]. The tracking parameters used have been tuned to those results. The shower particles are followed individually down to 100 keV, the saturation effects in the scintillator are taken into account reducing the recorded energy deposition signal by the Birks factor. Neither light attenuation in the scintillator, light collection effects, nor effects of photoelectron statistics, are included in the simulation.

The EM and HAD sector are intercalibrated with just one single calibration constant, independent of the incoming particle energy. No major improvement has been observed making use of a π^0 weighting technique [13] of the 4 individual hadronic longitudinal samplings. This calibration constant can be obtained in two ways : either minimizing the overall energy resolution or making the energy response independent of the fraction of energy measured by the EM part alone. The intercalibration between preshower detector and EM calorimeter is calculated with electrons.

4.1 Energy resolution and linearity of the response

Light quark jets from 40 to 1000 GeV have been passed through the hybrid calorimeter system. The resolution values are fitted best by the functional form

$$\frac{\sigma^{jet}}{E} = \frac{(27 \pm 2)\%}{\sqrt{E(GeV)}} + (1.2 \pm 0.2)\%$$

where the quoted errors are purely statistical. Fig. 10 shows the dependence of the resolution on the initial jet energy, as well as the fit result. On the same figure a fit to the response of single pions is presented. In this case the sampling term of the resolution function is increased to about 40%. The dependence of the overall resolution from the longitudinal depth of the calorimeter has also been studied. For 300 GeV jets the resolution saturates at about $7 \lambda_I$ inside the hadronic section (in our case about 140 cm of calorimeter thickness), which corresponds to about $9 \lambda_I$ for the total calorimeter. Fig. 11 shows the energy dependence of the response normalized to 1 at 100 GeV. Although the intercalibration factor has been kept constant, i.e. energy independent, the linearity stays within $\pm 2\%$.

First simulations have also been performed to study the effect of random tile-to-tile light yield fluctuations. For jets these fluctuations can reach an RMS of 20 % without significantly increasing the constant term in the energy resolution.

4.2 Effect of dead materials

The presence of a cryostat structure just in front of the hadronic section implies a substantial amount of passive absorber material, which might be a source of systematics and tails. The simulation shows that at $\eta = 0$ a 150 GeV jet loses on average 3.3 GeV in this dead material, with an RMS of 2.3 GeV. This induced energy fluctuation has to be compared to the 6.2 GeV of fluctuation expected in the calorimeter.

This material effect would be more substantial at larger η 's, for example at the edge of the barrel, where about $3 X_0$ of passive absorber material must be taken into account.

This effect has been studied, varying in the simulation the amount of material in between the two calorimeters from 0 to $3.2 X_0$ and looking at the variation of the resolution of 300 GeV jets. Fig. 12 shows such a dependence, where the middle point ($1.6 X_0$) reflects the situation at $\eta = 0$, and the point at $3.2 X_0$ the edge of the barrel calorimeter. Assuming that in the worst case this effect would give a contribution which is energy independent, it would result in an increase of about 0.5% in the constant term of the resolution function. No obvious abnormal tails are observed in the energy distributions.

5 Proposed parameters of a test module

Beam tests shall check the predicted properties of a large calorimeter as proposed for ATLAS. In addition the construction methods envisaged should be tested as far as possible. The design parameters of the test module are, therefore, closely linked to the ones of the barrel structure. We intend to build three sector modules of the width and depth corresponding to the design of the ATLAS barrel sector but with an active length of 1 m instead of 6.8 m. The tiles will have 100 mm height and will be arranged in 18 layers, alternately staggered. In depth a fourfold segmentation of the readout will be applied combining respectively 3, 4, 5, and 6 layers of tiles. In axial (z-) direction the sectors will have five readout cells. There will be an independent left and right readout of the tile edges. This structure leads to 40 readout channels for each of the three sectors. Each sector will have a weight of about 3.5 t. The three sectors mounted side by side will have an entrance face of $0.6 \times 1 \text{ m}^2$.

In order to compare the response of tiles from the two different production options two sectors will be equipped with injection moulded tiles and the third one with conventionally produced tiles. The readout will be performed with ex-UA2 PMTs.

6 The R&D Program

6.1 Construction of the calorimeter test module

The aim is to construct a test module consisting of three sectors described in Sec.5. The steps are :

- cutting and drilling of the absorber plates (1.5 and 2 mm thick),
- assembly of the absorber stacks and welding of the outside structures,
- injection and/or cutting and drilling of the scintillator tiles,
- wrapping of the scintillator tiles and mounting them into the sectors,
- preparation (cutting, polishing, aluminium mirroring of the end-faces) of the WLS-fibers,
- insertion, bundling and glueing of the fibers for each readout channel and machining and polishing of the fiber bundle end faces,
- mounting and cabling of the PMTs.

6.2 Preparation of the test beam setup and beam tests

First tests are envisaged in the H2 beam, using different energies of pions, muons, and electrons. In a second test period the test module should be installed behind the existing liquid argon calorimeter prototype of RD3 in the H8 beam. All test data will be compared with the corresponding simulations. The test beam results will provide information to the following questions :

- Does the energy resolution correspond to the simulations ?
- Is the effect of local fluctuations of light production and light transfer as small as predicted by the simulations ?
- Is the use of injection moulded scintillator tiles adequate for good calorimeter performance ?
- What is the actual light yield (number of photoelectrons per incident GeV) ?

6.3 Light detector testing and developments

These studies are oriented towards a large calorimeter system in the ATLAS environment. They include both options : PMTs and APDs. This part of the program consists of :

- testing of small size PMTs and green extended photocathodes,
- the optimization of the magnetic shields for PMTs,
- for PMTs the design of the high voltage distribution with individual gain adjustment,

- the study of new APDs with reduced area,
- for APDs the design of a local HV-supply to be mounted close to each detector,
- for APDs the design of the associated fast preamplifier,
- the study of a calibration system (light pulser) to monitor the sensitivity of the light detectors.

6.4 Light detector mounting scheme

In the ATLAS environment it will be very desirable to have the possibility of accessing the light detectors without removing the surrounding muon chambers. A possible concept for the light detector mounting in the barrel calorimeter could be the installation, on each half sector module, of a pair of drawers (each 170 cm long) coupled in series and moving along the z-direction (Fig. 13). Each drawer should contain the light detectors and, in the case of APDs, the associated electronics, including possibly the front-end, the temperature probes, and the slow control. The drawers will also have to provide the cooling, which in the case of APDs despite their low power consumption is needed for the temperature stabilization. The design of such a system with particular emphasis on the problem of a reproducible light coupling of the light detectors to the WLS-fiber bundles is included in the development program.

6.5 Simulation program

Further simulations will concentrate on the following aims :

- optimization of the design parameters,
- development of energy calibration procedures,
- simulation of the beam test conditions,
- study of radiation effects on the calorimeter performance.

6.6 Component tests and radiation damage studies

Various tests, including radiation hardness measurements, are envisaged to measure the properties of :

- the scintillator tiles,
- the WLS-fibers,
- the tile-fiber coupling efficiency (design optimization).

In addition the radiation hardness of a hadron calorimeter module will be tested in a high energy beam at CERN.

6.7 Engineering studies

Further engineering studies will concentrate essentially on the overall design aspects, including a detailed cost evaluation in collaboration with industry, and on the installation scenario in the ATLAS environment.

6.8 Time scale

The time scale foreseen is shown on Table 2. An obvious milestone will be the first beam test of the test module. The results will be an important input for the decision of the ATLAS Collaboration on the calorimeter option to be retained. This decision is intended to be taken by July 1993.

6.9 Budget

	1993	1994
	KSF	KSF
Test module construction	135	
Test module improvements	20	35
H2-beam installation	25	
H8-beam installation	10	40
Light detector developments	110	40
Engineering studies	60	60
	360	175

Cost sharing	1993	1994
Barcelona	30	50
Bucharest	20	
CERN	120*	40
Clermont-Ferrand	175	40
IHEP	10	5
Lisbon		30
Prague	5	10

(*) Already included in the ATLAS CERN budget request.

6.10 Sharing of responsibilities

- Test module construction :
Barcelona, Bucharest, CERN, Clermont-Ferrand, IHEP, Lisbon, Yerevan
- Test beam installations :
CERN, Clermont-Ferrand
- Beam tests :
Barcelona, Bucharest, CERN, Clermont-Ferrand, IHEP, Lisbon, Prague, Yerevan
- Simulations and analysis :
Barcelona, CERN, Clermont-Ferrand, Lisbon
- Component tests :
CERN, IHEP, Lisbon, Prague
- Light detector development :
Clermont-Ferrand

- **Engineering studies :**
Bucharest, CERN, Clermont-Ferrand
- **Calibration :**
Barcelona, CERN, Clermont-Ferrand, Lisbon

References

- [1] Proceedings of the Second International Conference on Calorimetry in High Energy Physics, Capri, 1991. J. Freeman *et al.*, page 189.
- [2] SDC Technical Report, SDC-92-201.
- [3] O. Gildemeister *et al.*, in [1], page 199.
- [4] ATLAS Letter of Intent, CERN/LHCC/92-4.
- [5] T. Camporesi *et al.*, in Proceedings of the NSS-IEEE Conference, Orlando, 1992.
- [6] Advanced Photonix, application note APHO-91-1, 1991.
- [7] The RD1 Collaboration, Recent results on APDs tests, in preparation.
- [8] D. Green *et al.*, in Proceedings of the International Conference on Radiation Tolerant Plastic Scintillators and Detectors, Tallahassee, 1992.
- [9] A. Beer *et al.*, Nucl. Instrum. Methods **A224** (1984) 360.
- [10] R. Brun *et al.*, GEANT 3.15, CERN Computer Newsl. **203** (1992).
- [11] V. Vercesi *et al.*, in [1], page 172.
- [12] E. Bernardi *et al.*, Nucl. Instrum. Methods **A262** (1987) 229.
- [13] H1 Calorimeter Group, W. Braunschweig *et al.*, DESY 89-022 (1989).

Figure captions

1. Schemes of the readout of scintillator tiles with WLS fibers, with conventional geometry (a), and longitudinal geometry (b).
2. Staggering of tiles in a module (schematic, not to scale).
3. ATLAS hybrid calorimeter layout.
4. Structural layout of a barrel module of the scintillating tile calorimeter.
5. R-z segmentation of the scintillating tile calorimeter.
6. Test of the fiber to tile optical coupling.
7. Light output (natural log scale) of a 2.2 m long WLS fiber as a function of the distance between the excitation point and the PMT. The fiber is aluminized at the end.
8. 40 GeV electrons response for a given impact point on the RD1 EM test module, with PMT readout (a), and with APD readout (gain of 20) (b).
9. APD electronic pulses as seen by a digitizing scope. Direct APD output from 150 GeV electrons (APD gain 50) (a), and from a laser pulse, after a fast current preamplifier (APD gain 20) (b).
10. Jet and single pion resolution and fit results (GEANT simulation, using FLUKA model), in the ATLAS hybrid calorimeter configuration.
11. Response linearity for simulated jets.
12. Dependence of the simulated jet energy resolution on the amount of material between EM and HAD compartments.
13. Schematic view of the drawers system moving along the z-direction.

moderator	5cm	0.06 λ_I
Coil + cryostat	7.8 cm Al + 0.2 cm Fe	0.22 λ_I
preshower	1.1 cm Pb + 6 cm LAr	0.14 λ_I
Accordion	support 4.cm Plast. + 2.6cm LAr	
	Pb + Fe 15 cm	
	LAr active 30 cm	1.32 λ_I
Cables + electr. + LAr	2 x 4 cm	0.09 λ_I
1 cm Fe as support		0.06 λ_I
+ outer cryostat	1 cm Fe + 3 cm Al	0.14 λ_I
	Total	2.0 λ_I

Table 1: Breakdown of materials in front of the HAD calorimeter.

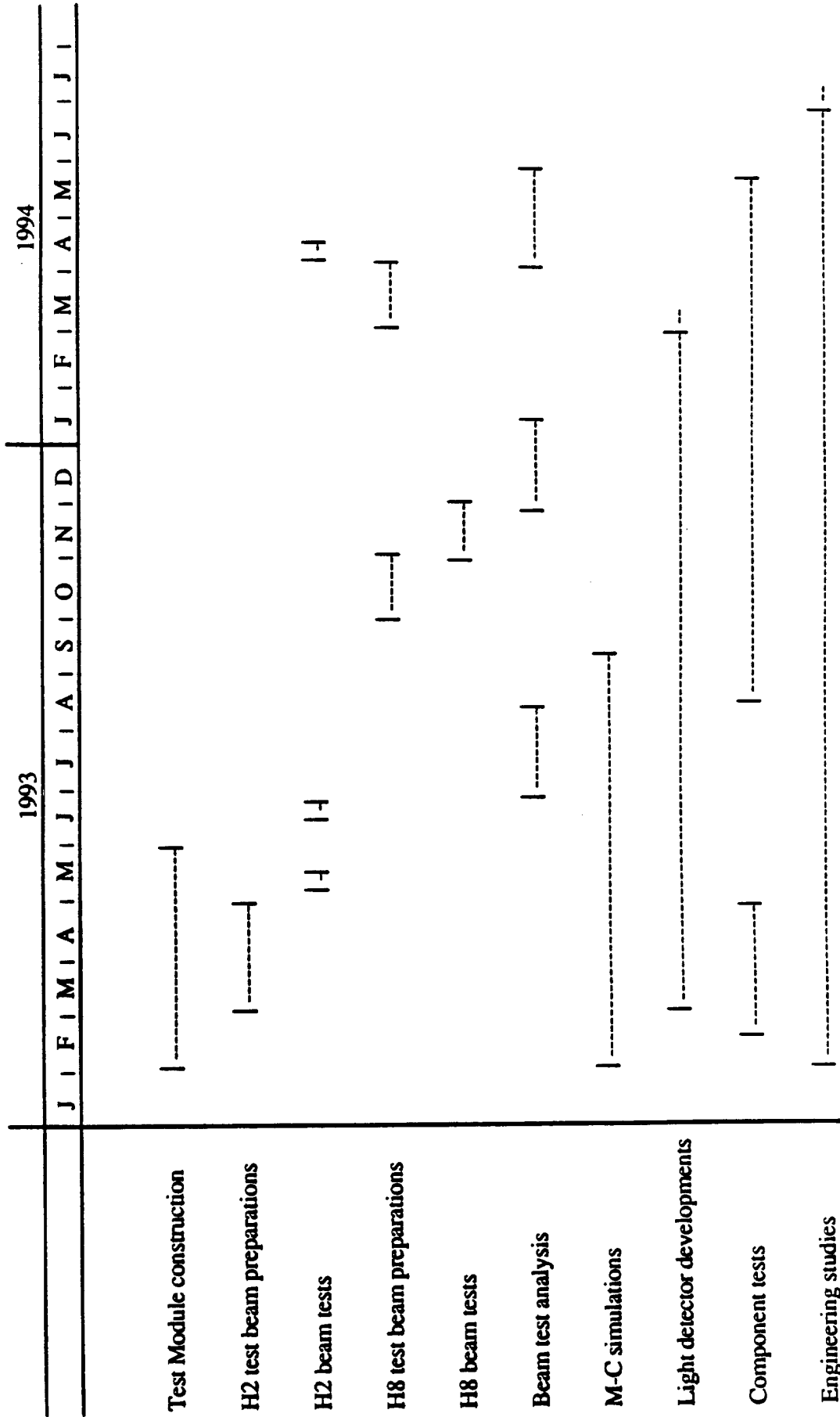


Table 2: Time scale.

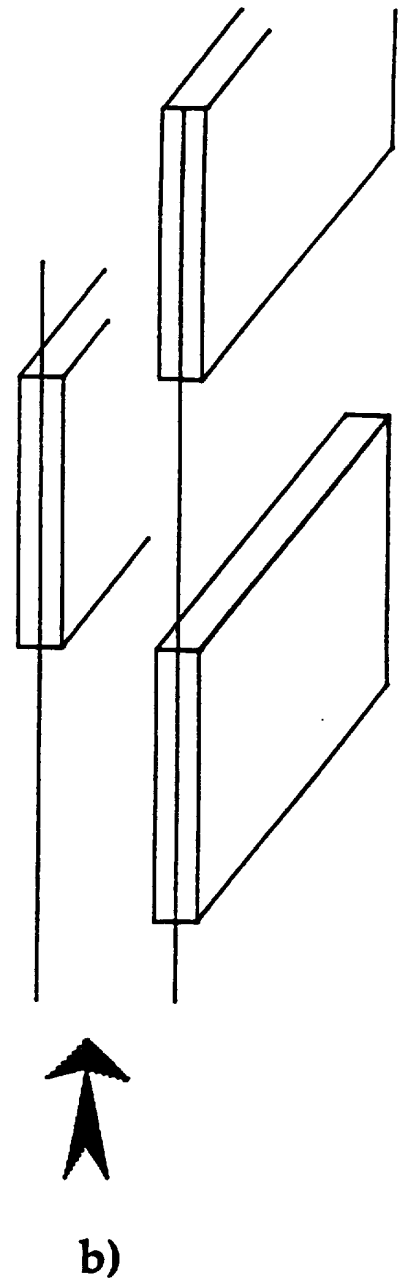
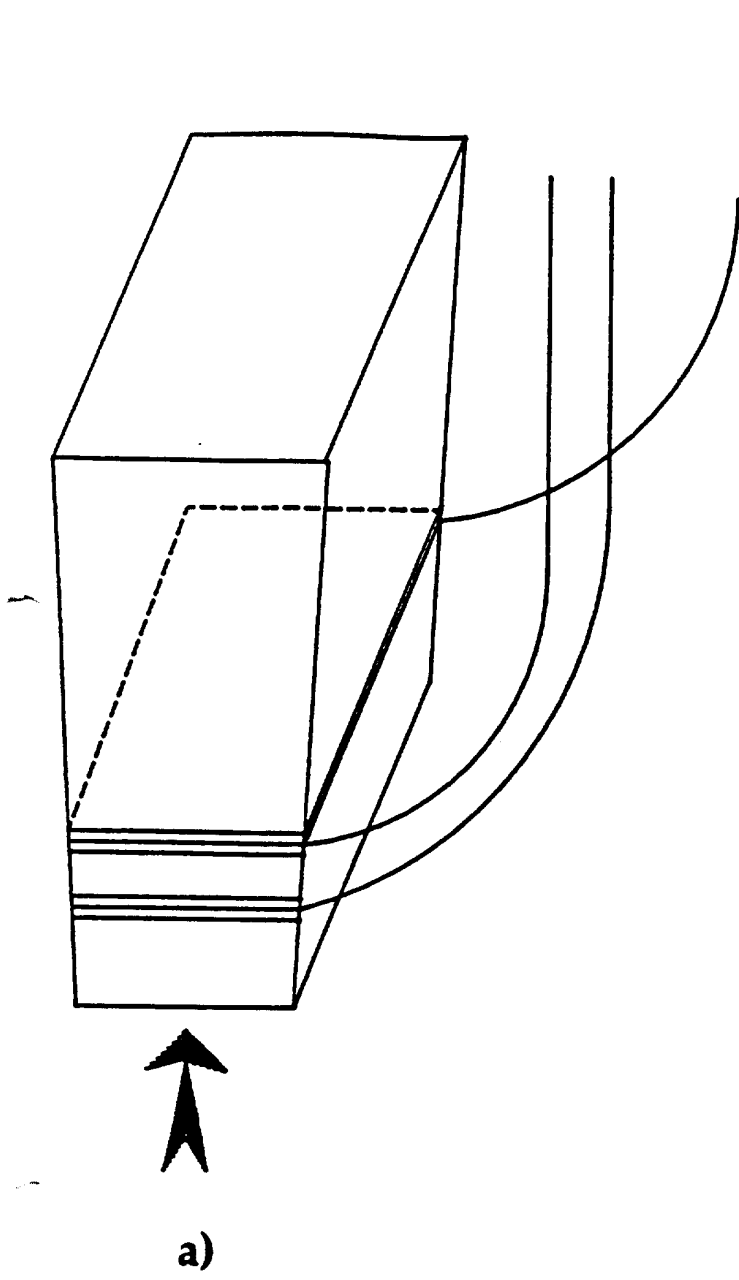


Fig. 1

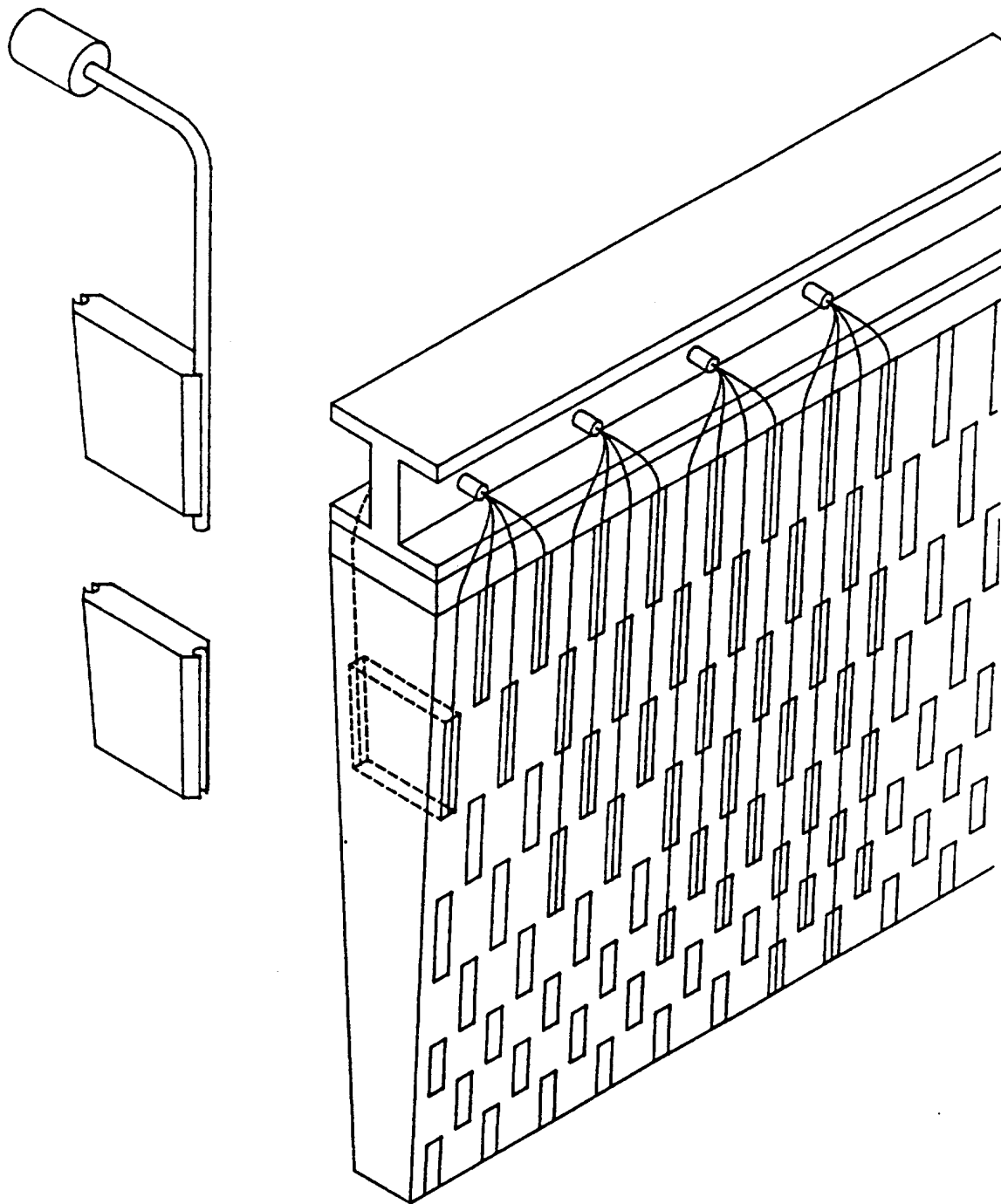


Fig. 2

6550

3450

B-Flux Return

Central Barrel

Extended Barrel

Calorimeter LAr

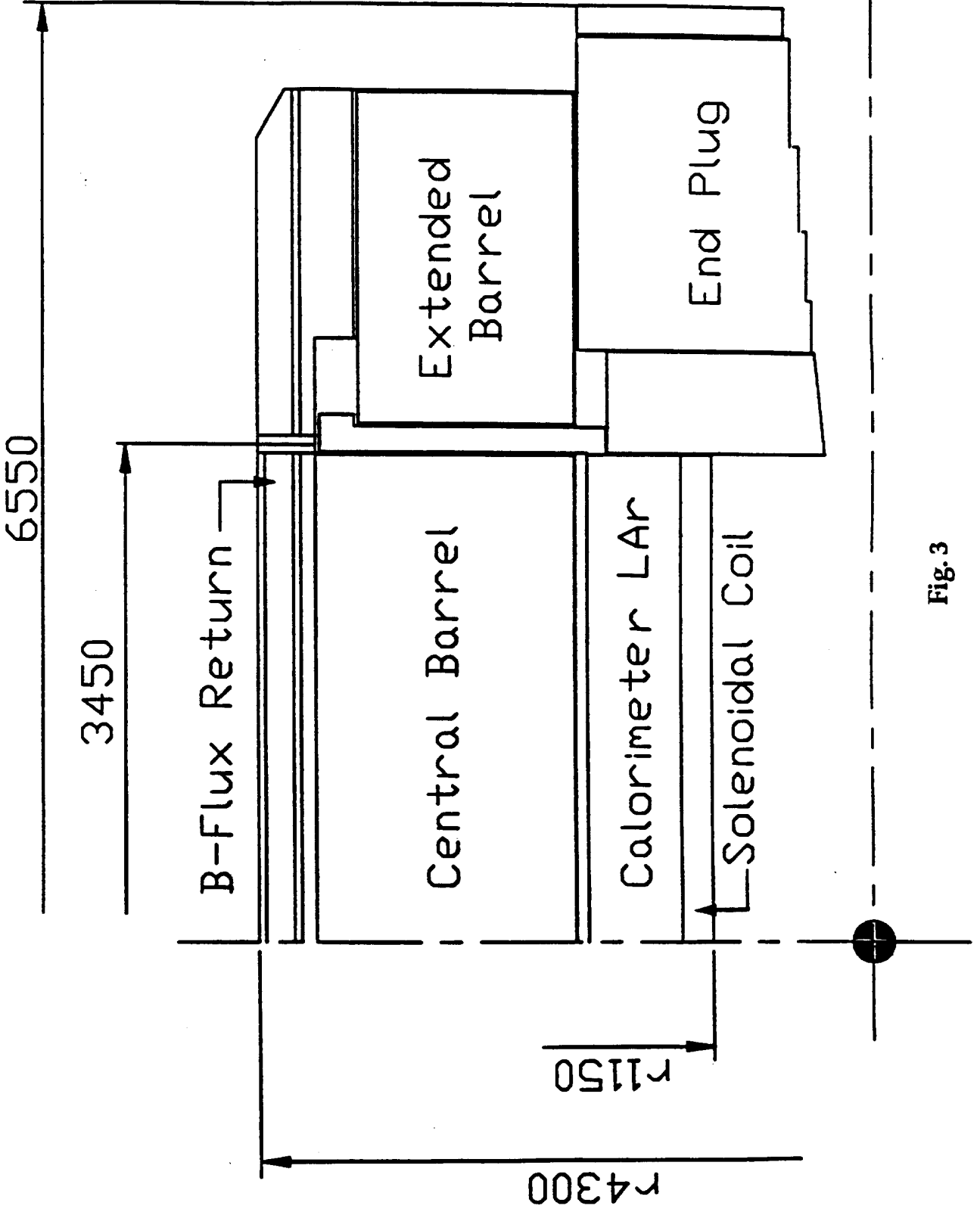
End Plug

Solenoidal Coil

R4300

R1150

Fig. 3



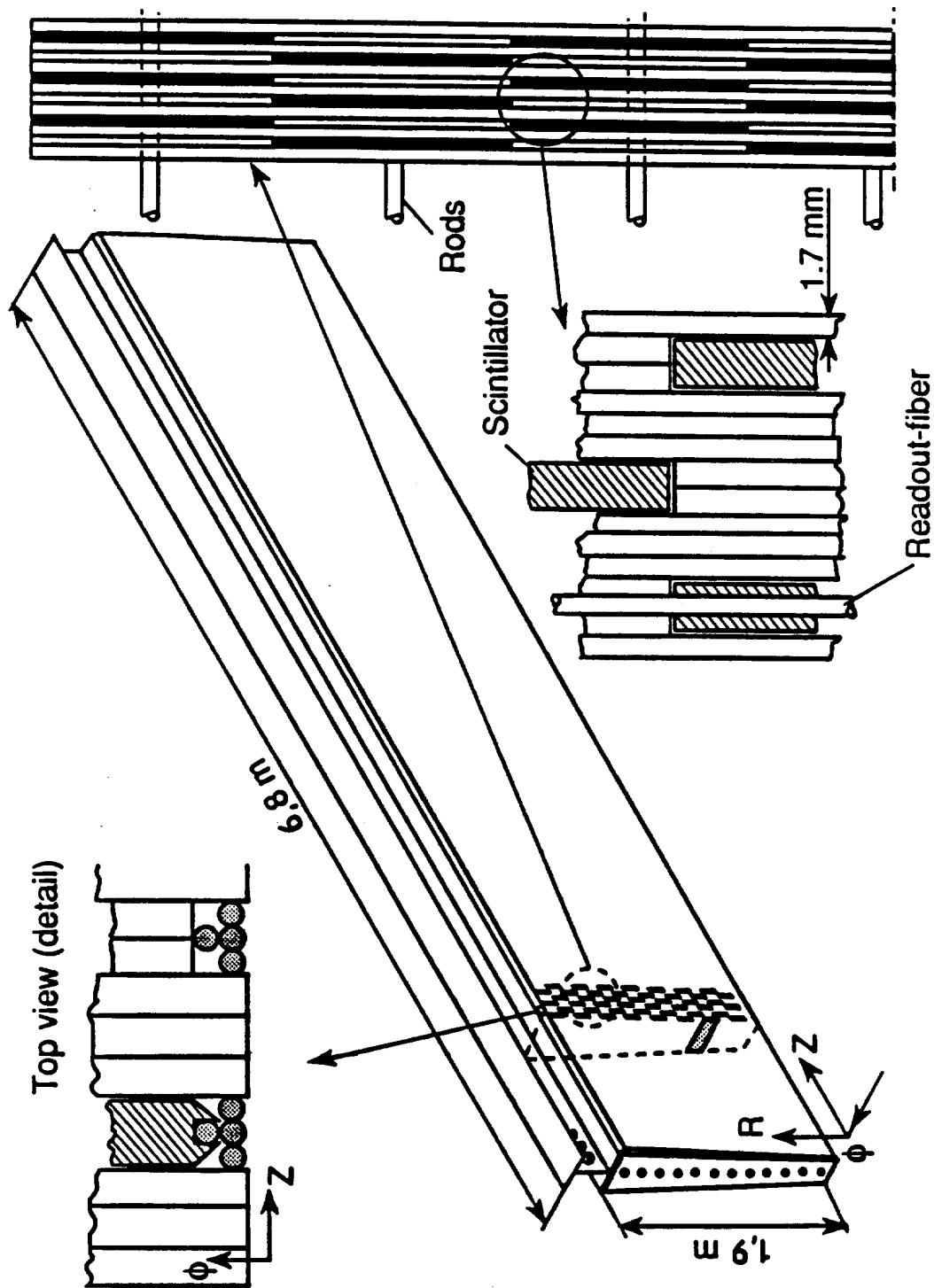


Fig. 4

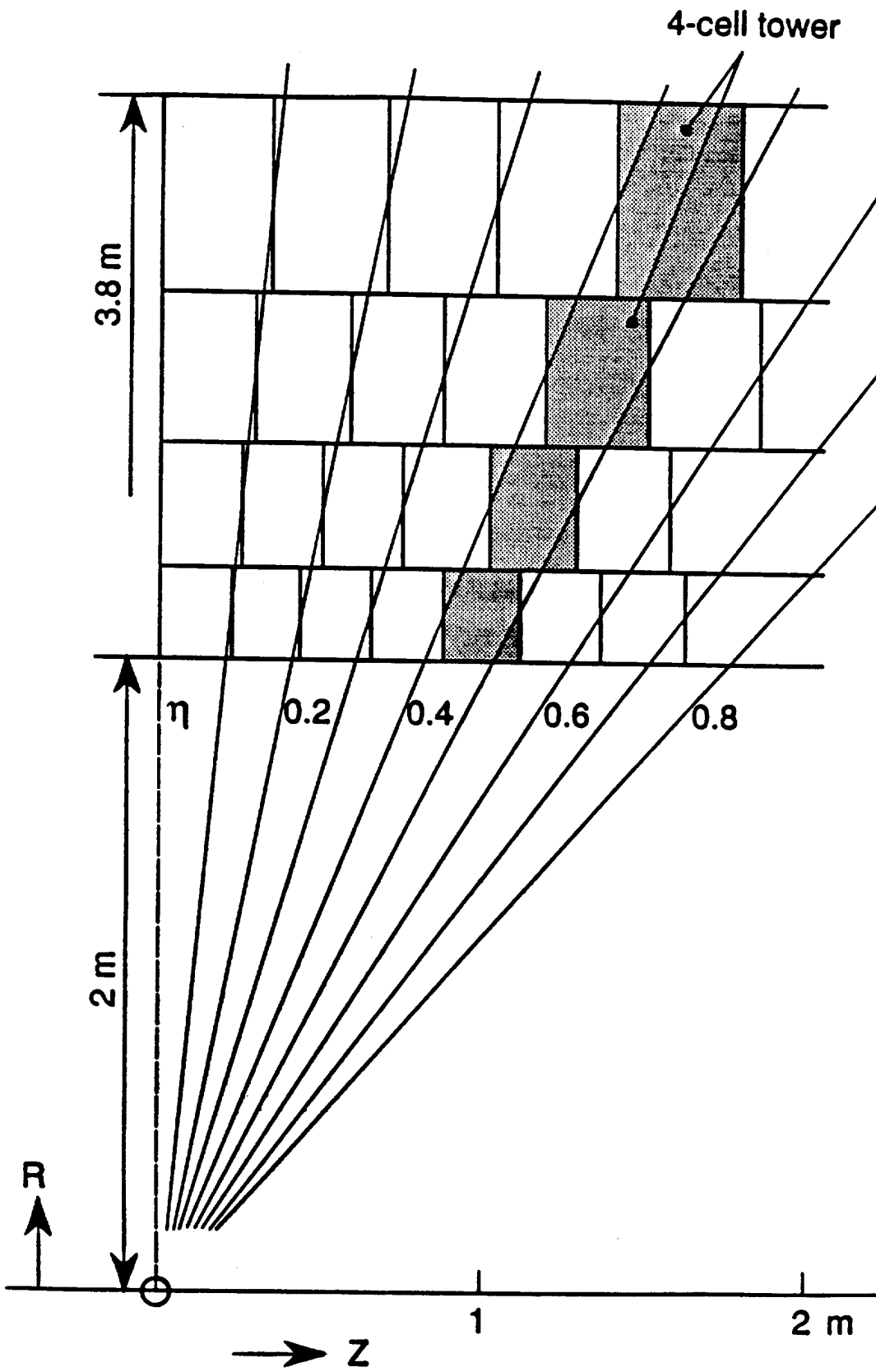


Fig. 5

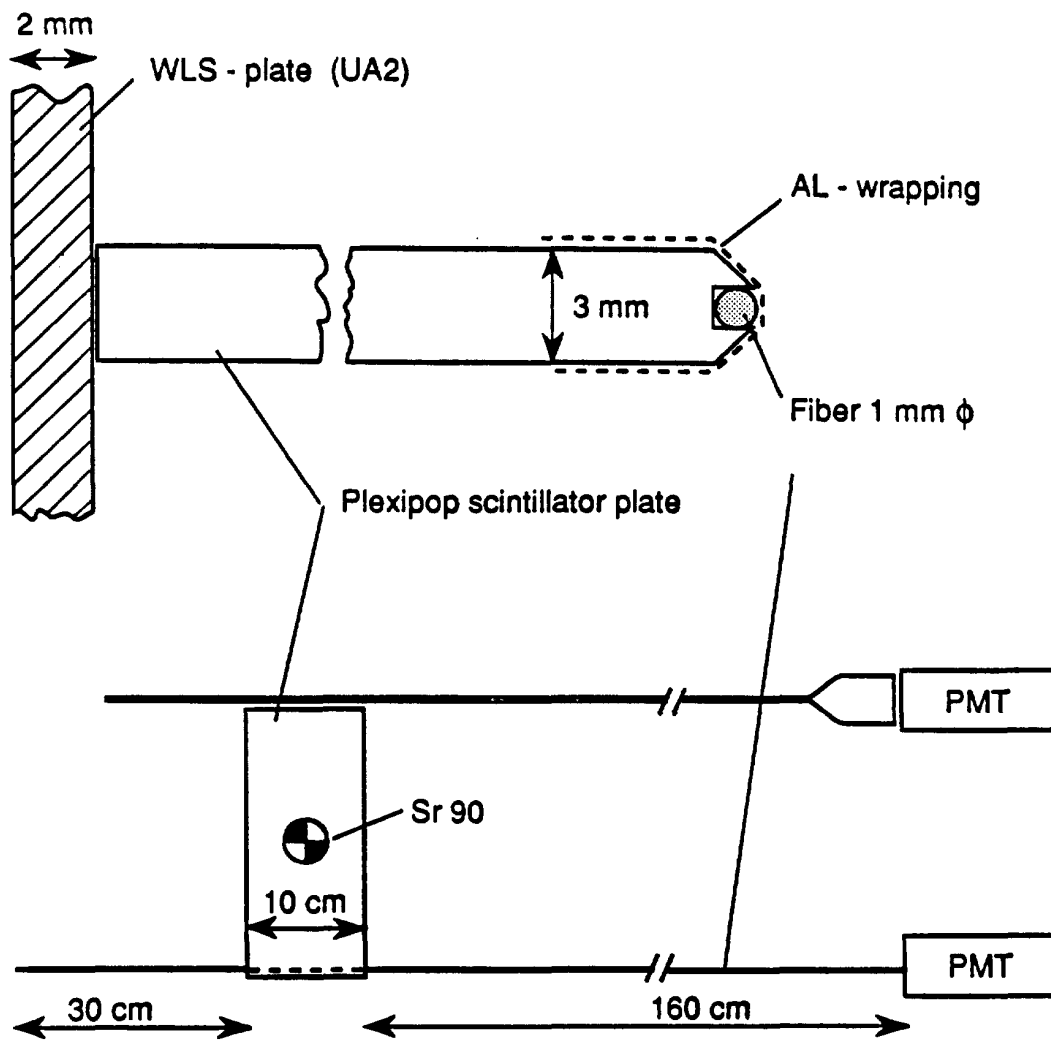


Fig. 6

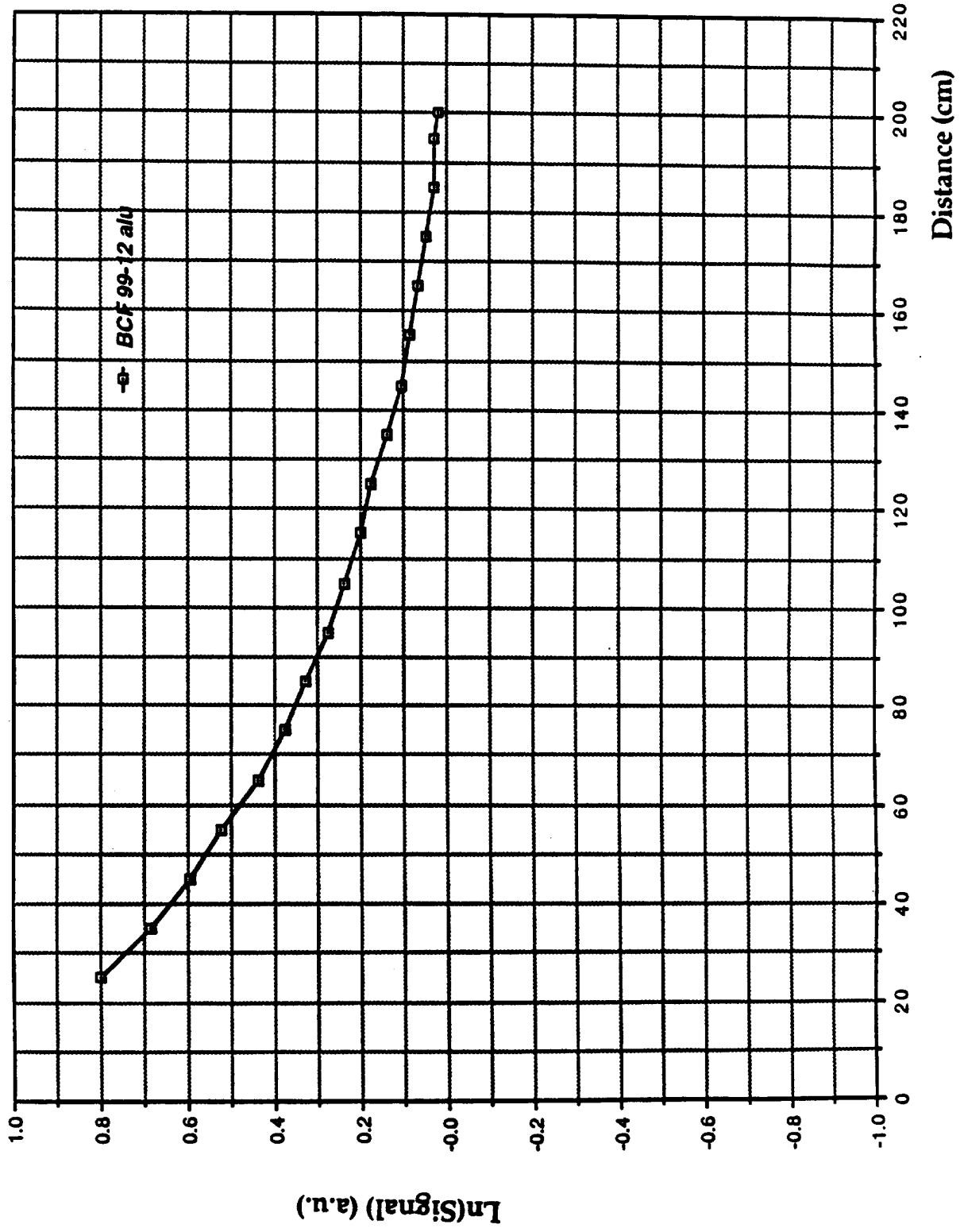


Fig. 7

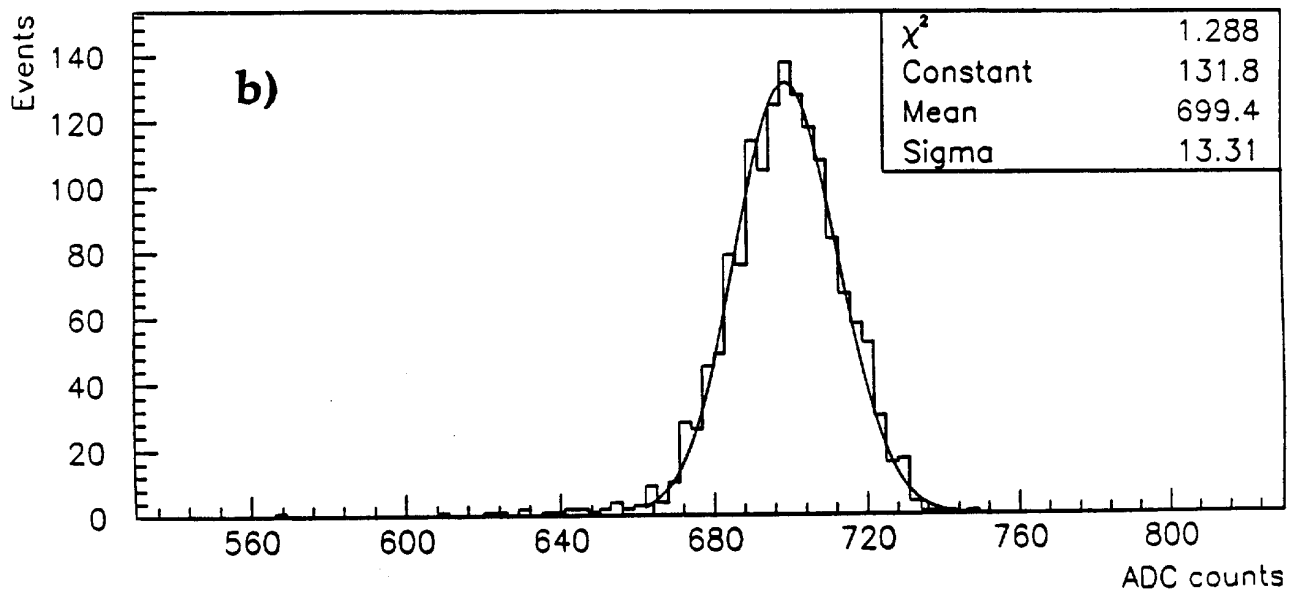
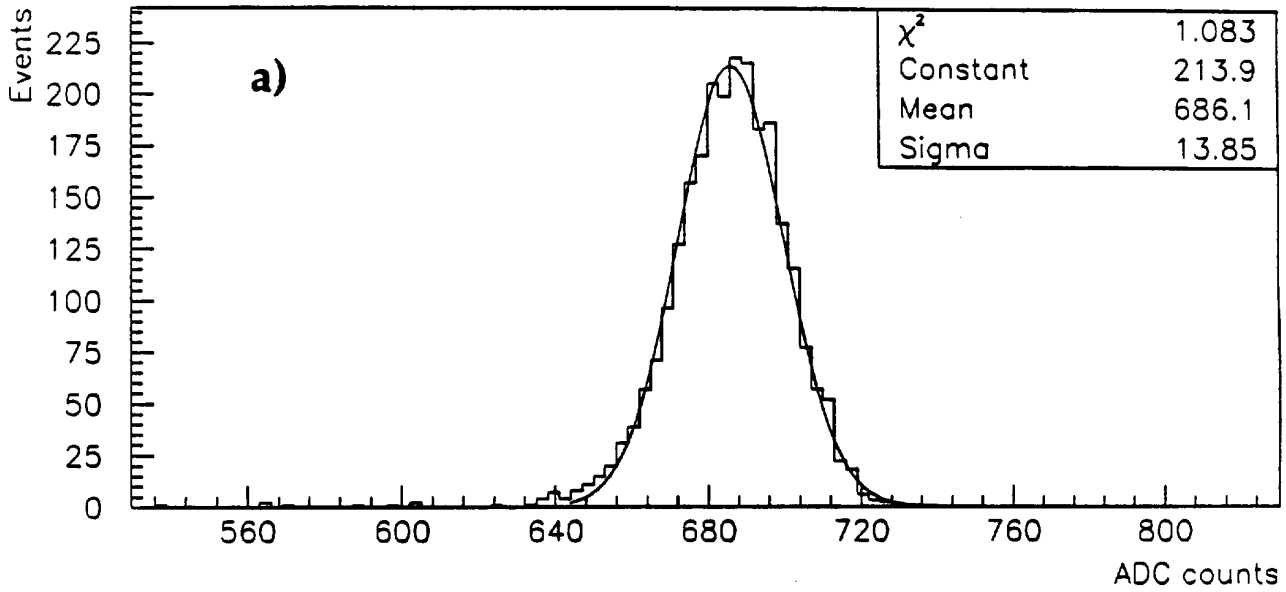
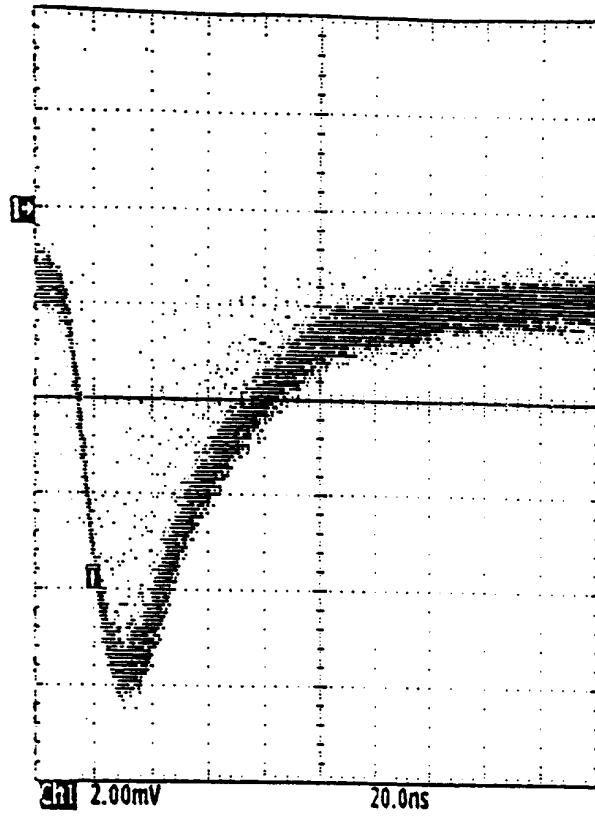
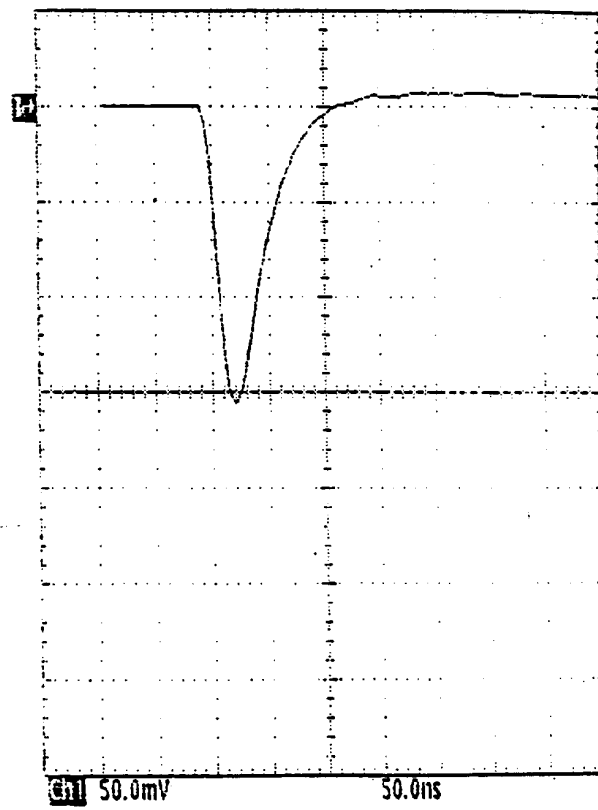


Fig. 8



a)



b)

Fig. 9

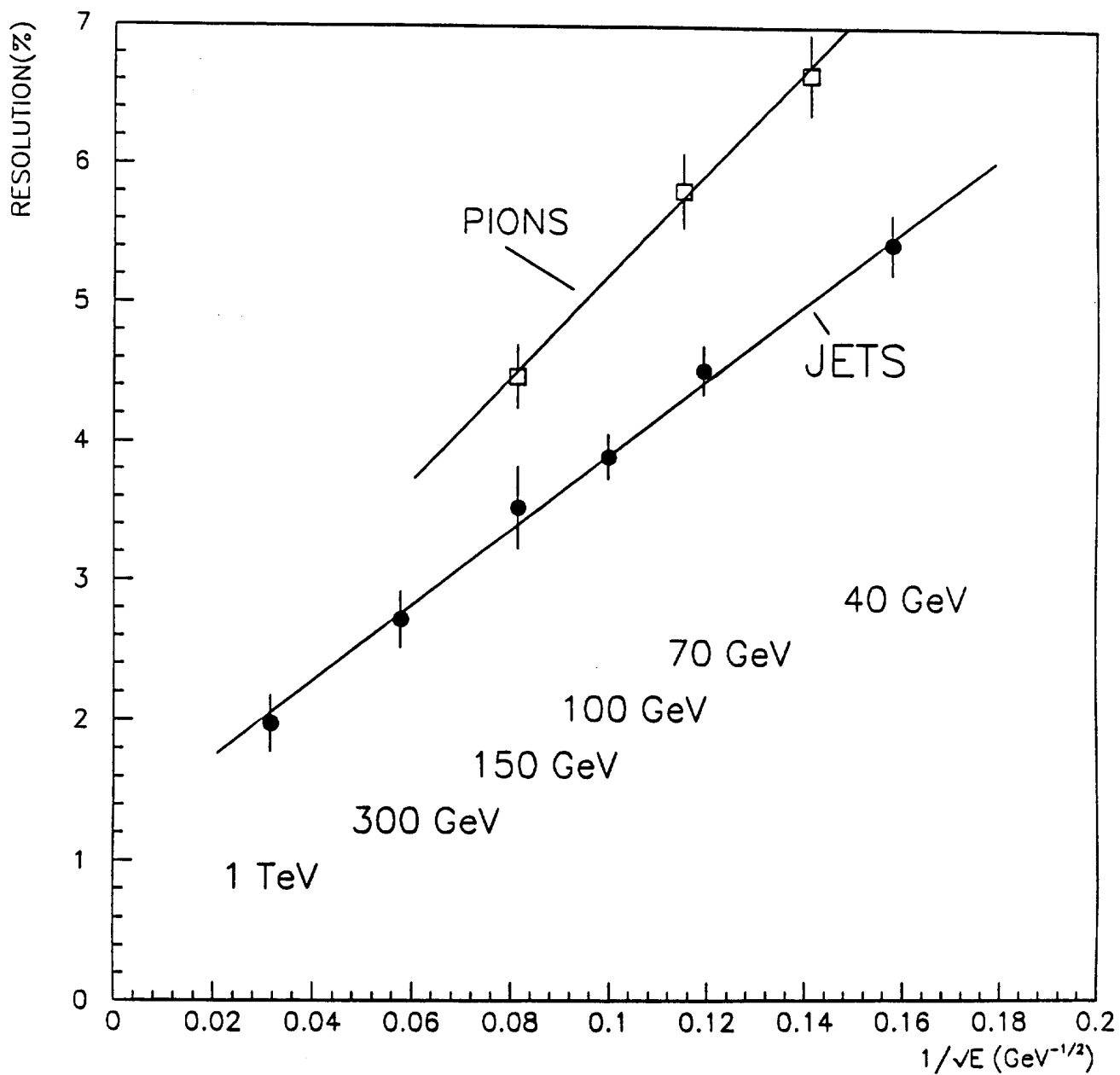


Fig. 10

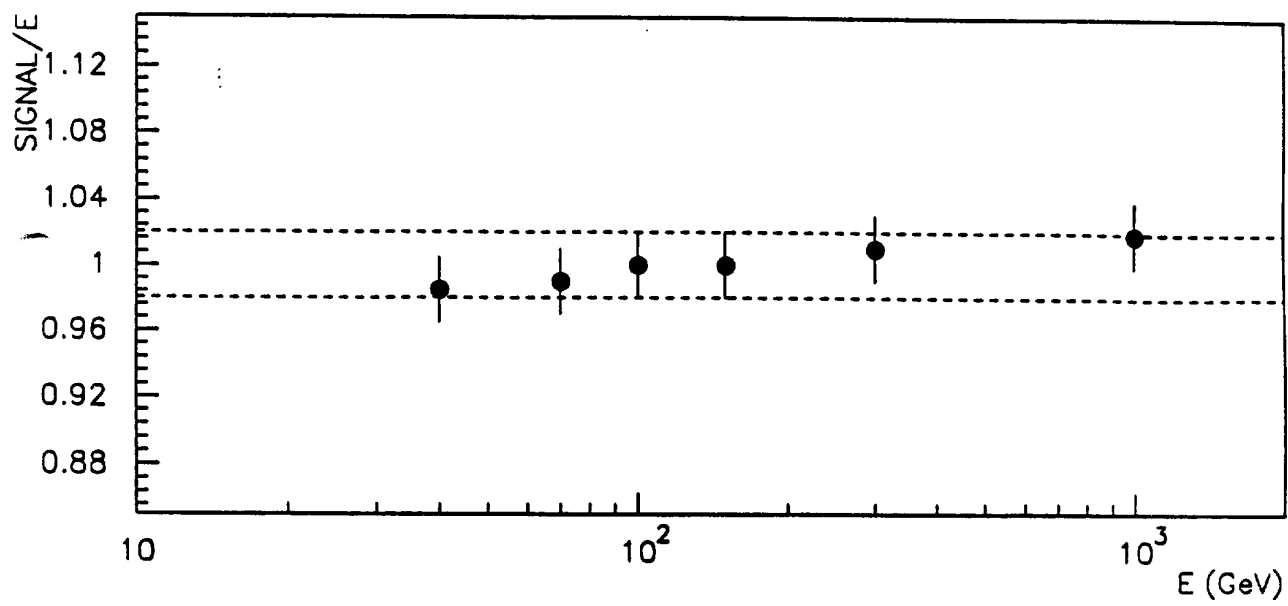


Fig. 11

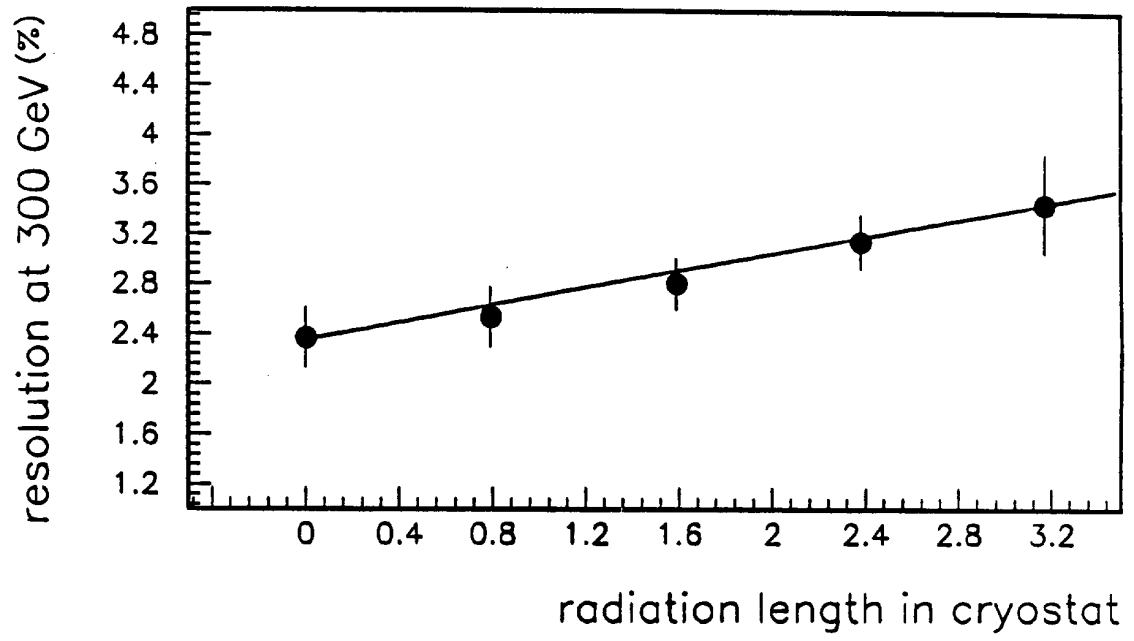


Fig. 12

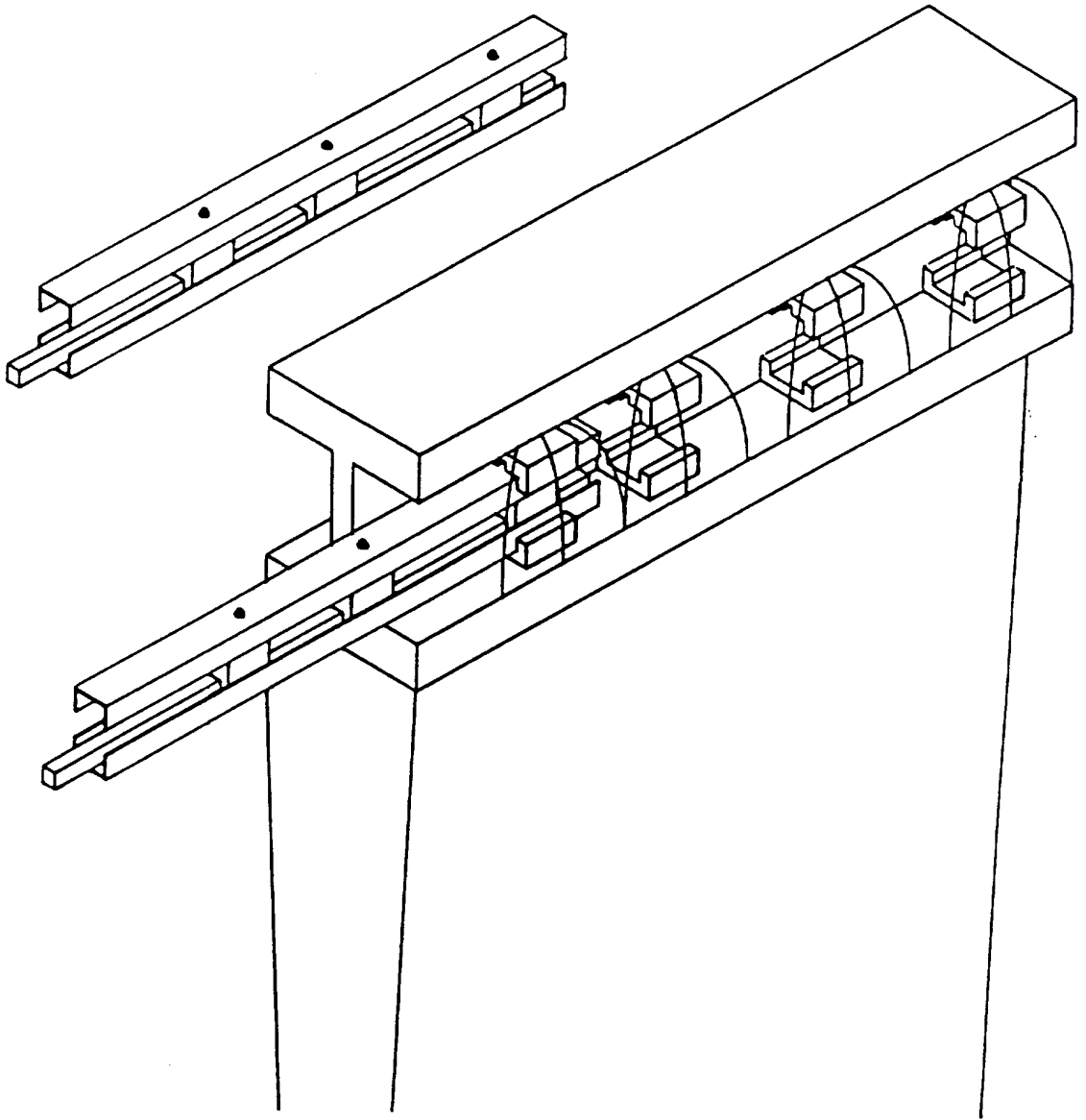


Fig. 13

